

On a Sparse Shortcut Topology of Artificial Neural Networks

Feng-Lei Fan¹, *Student Member, IEEE*, Dayang Wang², Hengtao Guo¹, Qikui Zhu¹, *Student Member, IEEE*, Pingkun Yan^{1*}, *Senior Member, IEEE*, Ge Wang^{1*}, *Fellow, IEEE*, and Hengyong Yu^{2*}, *Senior Member, IEEE*

Abstract—Over recent years, deep learning has become the mainstream data-driven approach to solve many important real-world problems. In the successful network architectures, shortcut connections are well established to take the outputs of earlier layers as additional inputs to later layers, which have produced excellent results. Despite the extraordinary effectiveness of shortcuts, there remain important questions on the underlying mechanism and associated functionalities. For example, why are shortcuts powerful? Why shortcuts generalize well? To address these questions, we investigate the representation and generalization ability of a sparse shortcut topology. Specifically, we first demonstrate that this topology can empower a one-neuron-wide deep network to approximate any univariate continuous function. Then, we present a novel width-bounded universal approximator in contrast to depth-bounded universal approximators, and also extend the approximation result to a family of networks such that in view of approximation ability, these networks are equally competent. Furthermore, we use the generalization bound theory to show that the investigated shortcut topology enjoys an excellent generalizability. Finally, we corroborate our theoretical analyses with experiments on some well-known benchmarks.

IMPACT STATEMENT

Shortcuts are the key elements of many well-performed neural network architectures, and have been achieved huge success in many applications. However, why shortcuts are powerful was not so much investigated in a theoretical point of view in the past years. To fill this gap, we present detailed analyses on how powerful a sparse shortcut topology is in views of expressibility and generalizability. Furthermore, our theoretical analyses are corroborated by comprehensive prediction and classification experiments. Our work is useful in understanding the role of shortcuts and can inspire more research in neural architecture design.

I. INTRODUCTION

Recently, deep learning [1] has been rapidly evolving and achieved great success in many applications [2]–[6]. Since AlexNet [7], more and more models were developed; for example, Inception [8], Network in Network [9], VGG [10], ResNet [11], DenseNet [12], and so on. These models play an important role as backbone architectures, pushing the performance boundaries of deep leaning on the downstream tasks.

*Drs. Pingkun Yan, Ge Wang and Hengyong Yu serve as co-corresponding authors. This work was partially supported by IBM AI Horizon Scholarship.

¹Feng-Lei Fan (fanf2@rpi.edu), Hengtao Guo, Qikui Zhu, Pingkun Yan and Ge Wang (wangg6@rpi.edu) are with Department of Biomedical Engineering, Rensselaer Polytechnic Institute, Troy, NY 12180, USA

²Dayang Wang and Hengyong Yu (hengyong_yu@uml.edu) are with Department of Electrical and Computer Engineering, University of Massachusetts, Lowell, MA 01854, USA

In these studies, great efforts were made to explore the use of skip connections [13]–[17]. For instance, a shortcut topology was searched in the framework of a lightweight network for a super-resolution task [13]. Hypercolumn Network [14] stacked the units at all layers as concatenated feature descriptors to obtain semantic information and precise localization. Highway Network [16] achieved great successes in training a very deep network. Fractal Network [17] utilized a different skip connection design, by which interacting sub-paths were used without any pass-through or residual connections.

In the 1990s, the universal approximation theorem was proved to justify the representation power of a network. Given a sufficient number of neurons, a one-hidden-layer network can express any continuous function [18], [19]. Recently, inspired by successes of deep learning, intensive efforts were put to explain the advantages of depth over width of a network. The basic idea behind these results is to construct a special class of functions that a deep network can efficiently represent but shallow networks cannot [20]–[24]. However, it is tricky that despite the incorporation of shortcuts greatly empowers a neural network in solving real-world problems, theoretical studies are few to explain the representation and generalization abilities of shortcuts. In this study, we present our theoretical findings on a novel sparse shortcut topology, wherein shortcuts are used to bridge all the previous layers and the final layer in the whole network or a block (see Figure 1), thereby shedding light on why shortcuts are effective machineries in machine learning.

First, we show that the one-neuron-wide network with the proposed topology can approximate any univariate function, while the one-neuron-wide feedforward network cannot. This suggests that adding shortcuts can lead to a more powerful network structure. Along this direction, we report an alternative novel width-bounded universal approximator by using the Kolmogorov-Arnold representation theorem [25], in contrast to the depth-bounded universal approximator [26]–[28]. The width-bounded universal approximator refers to the universal approximators whose width is limited but depth is arbitrarily large, while the depth bounded universal approximators have a limited depth, but its width can be arbitrarily large. Given the input of n dimensions, the required width is no more than $2n^2 + n$ per layer in our scheme. Then, we extend the result to a family of networks such that in view of approximation ability, these networks are equally competent. Furthermore, we analyze the effect of concatenation shortcuts on the generalization bound of deep networks, and show that the investigated topology enjoys a tighter generalization bound compared with the densely

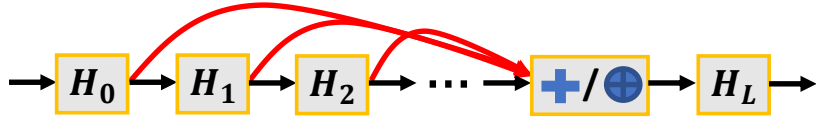


Fig. 1. A novel sparse shortcut topology. There are two aggregation approaches: summation and concatenation. In the following, we denote summation and concatenation as $+$ and \oplus , respectively.

connected one, which suggests that the investigated topology can generalize well. To verify the positive results from the theoretical analyses, we prototype a network with the proposed topology and evaluate its performance on some well-known benchmarks. Finally, the experimental results demonstrate that the constructed network can achieve competitive learning performance in comparison with networks with residual topologies, the densely connected network, and other state-of-the-art models.

In summary, our contributions are three-fold. 1) We demonstrate the expressibility of the shortcut connections by presenting a univariate continuous function approximation theorem and a width-limited universal approximator, which partially addresses why networks with shortcuts are powerful. 2) To the best of our knowledge, our work is the first to analyze the generalizability of concatenation shortcuts based on the generalization bound theory. In addition, we also show that generalization bounds of the proposed topology are tighter than those of the densely connected topology. 3) We conduct experiments to validate our theoretical analyses, and the investigated topology performs competitively in regression and classification experiments on several well-known benchmarks.

To clarify, all our studies are based on the architecture shown in Figure 1, which is a special type of skip connections. The central hypothesis of this paper is that the proposed topology in Figure 1 enjoys a good expressibility (Section III) and generalizability (Section IV). Because the core of the proposed topology is the employment of shortcuts, our work also explains why shortcuts are important in a network structure. This hypothesis is validated by comprehensive experimental comparisons (Section V).

II. RELATED WORK

There are studies to explain the success of summation shortcuts. It was reported in [28] that with residual connections, one neuron is sufficient for the ResNet to approximate any Lebesgue-integrable function. In [29], it was showcased that the residual networks demonstrate an ensemble-like behaviour. Liu *et al.* [30] studied the convergence behavior of a two-layer network and proved that the optimization of a two-layer ResNet can avoid spurious minima under mild restrictions. He *et al.* [31] studied a spectrally-normalized margin bound to discuss the influence of residual connections on the generalization ability of deep networks. They showed that the margin-based multi-class generalization bound of ResNet is of the same magnitude as that of chain-like counterparts. Therefore, the generalizability of ResNet is not worse than that of feedforward networks. Here, we not only justify the representation ability of summation

shortcuts, but also conduct the generalization bound analysis for concatenation shortcuts, which systematically enrich our understanding to the expressibility and generalizability of shortcuts.

The work closely related to ours was done in [32], [33], which utilized the proposed network topology (Figure 1) as a backbone for CT image denoising and super-resolution. However, their studies were not theoretical and did not answer why such a structure can work. In contrast, we approach the utility of this shortcut topology through detailed mathematical analyses and comprehensive experiments. In addition, the investigated topology here is a sparsified version of the densely connected shortcut topology. By setting the relevant weights as zero, the densely connected topology will reduce into the topology here. Our results somehow show that the densely connected topology is redundant.

As far as the universal approximation is concerned, in Lu *et al.* [26], giving at most $n + 4$ neurons per layer and allowing an infinite depth, a fully-connected deep network with ReLU activation functions can approximate a Lebesgue-integrable n -dimension function accurately in the L^1 -norm sense. As an extension, Lin *et al.* [28] compressed $n+4$ into 1 by using residual connections. They also argued that because the identity mapping should be counted as n units, the actual width of their network is $n + 1$. Along this direction, we exploit the Kolmogorov-Arnold representation theorem [25] to derive a novel width-limited universal approximator with width no more than $2n^2 + n$ per layer. Although the upper bound of width in our universal approximator is greater than those set by [26] and [28], our work is still valuable because of the novelty of the methodology and the scarcity of width-bounded universal approximators.

III. EXPRESSIBILITY

In this section, we first study the representation ability of shortcut topology shown in Figure 1 that is based on summation ($+$) aggregation by presenting its superior approximation ability and then extend the results to more shortcut topologies, thereby shedding light on the question why shortcuts are powerful.

A. Univariate continuous function approximation

Our main result is that adding shortcuts, as shown in Figure 1, can make a one-neuron wide network approximate any univariate continuous function in the sense of the L^∞ distance. Mathematically, we make the following conjecture:

Conjecture 1: With ReLU activation functions for all neurons, for any continuous function $g : [0, 1] \rightarrow \mathbb{R}$ and any given precision $\delta > 0$, there exists a neural network G

of the proposed topology and one neuron in each layer such that

$$\sup_{x \in [0, 1]} |g(x) - G(x)| < \delta \quad (1)$$

The sketch of our constructive analysis: Any univariate continuous function can be approximated by a continuous piecewise linear function within any given closeness [34]. Therefore, the key of proof becomes how to implement this piecewise approximation by a one-neuron-wide network of the proposed topology. In our scheme, we use the ReLU as activation functions for all neurons except the output neuron. By convention of regression tasks, the activation function of the output layer is linear. Our construction is to make each neuron represent a piecewise function, and then we use shortcuts to aggregate these piecewise linear segments over intervals of interest in the output neuron.

Preliminaries: Without loss of generality, a continuous function $g(x)$ can be approximated by a continuous piecewise linear function $f(x)$ at any accuracy in the L^∞ sense, provided that the interval $[0, 1]$ is partitioned into very tiny sub-intervals. Therefore, to demonstrate the correctness of **Conjecture 1**, we just need to use a one-neuron-wide network of the investigated topology to implement $f(x)$. Suppose that there are N pieces in $f(x)$, we can construct an explicit expression of $f(x)$ as follows:

$$f(x) = \begin{cases} f_0(x) & x \in [x_0, x_1] \\ f_1(x) & x \in (x_1, x_2) \\ \vdots & \\ f_{N-1}(x) & x \in (x_{N-1}, x_N] \end{cases}, \quad (2)$$

where $x_0 = 0$, $x_N = 1$, and

$$f_i(x) = \begin{cases} \frac{f(x_{i+1}) - f(x_i)}{x_{i+1} - x_i}(x - x_i) + f(x_i) & x \in [x_i, x_{i+1}] \\ 0 & x \notin [x_i, x_{i+1}] \end{cases} \quad (3)$$

for $i = 0, 1, 2, \dots, N-1$, satisfying continuity. Hereafter, we use $M_i = \frac{f(x_{i+1}) - f(x_i)}{x_{i+1} - x_i}$ for simplicity. By default, neighboring segments should have different slopes, otherwise they will be combined as one segment.

Analysis: Now, let us show how to select parameters of a one-neuron-wide network to express $f(x)$ in the form of Eq. (2). The outputs of neurons are respectively denoted as $R_0, R_1, R_2, \dots, R_{N-1}$. For the i^{th} neuron, its output R_i is expressed as

$$R_i = (W_i x + b_i)^+, \quad (4)$$

where $(\cdot)^+$ denotes the ReLU operation, W_i and b_i are the weight and bias respectively. In the following, mathematical induction is used to show that our construction can express $f(x)$ exactly.

Initial Condition R_0 : We use R_0 to implement the linear function in the first interval $[x_0, x_1]$ referring to Eq. (3). By setting $W_0 = |M_0|$, $b_0 = -|M_0| x_0$, the specific function of the first neuron becomes $R_0 = (|M_0| (x - x_0))^+$, where the ReLU keeps the linearity when $x > x_0$.

Recurrent Relation: Suppose that we have obtained the desired i^{th} neuron R_i , we can proceed to design the $(i+1)^{th}$ neuron with the goal of expressing the function $|f_{i+1}(x) - f_{i+1}(x_{i+1})|$, which is $|f_{i+1}(x)|$ over the interval $(x_{i+1}, x_{i+2}]$ without a constant lift. The tricky point is that the current neuron basically takes in the output of the previous neuron as the input, which is in the functional range instead of the input domain. Therefore, we need to perform an inverse affine transform:

$$R_{i+1} = \left(|M_{i+1} - M_i| \times \left(\frac{1}{|M_i - M_{i-1}|} R_i - x_{i+1} + x_i \right) \right)^+ \quad (5)$$

For notation completeness, $M_{-1} = 0$. The trick we use is to invert R_i back to the input domain and set the new slope as $|M_{i+1} - M_i|$, which cancels the effect of R_i imposed on $x > x_{i+1}$, equivalently limiting R_i to only work over $(x_i, x_{i+1}]$ once R_i and R_{i+1} are added together. The parameters in the $(i+1)^{th}$ module are chosen as follows: $W_{i+1} = \frac{|M_{i+1} - M_i|}{|M_i - M_{i-1}|}$ and $b_{i+1} = (-x_{i+1} + x_i)|M_{i+1} - M_i|$.

Thanks to the recurrent relation, we can compute each R_i as $(|M_i - M_{i-1}|(x - x_i))^+$. We aggregate the outputs of those N pieces in the final neuron through shortcut connections to get the neural network $G(x)$ in Eq. (1) as follows:

$$G(x) = \sum_{i=0}^{N-1} sgn(i) R_i + f(x_0), \quad (6)$$

wherein $sgn(i) = 1$ when $M_i - M_{i-1} > 0$ and $sgn(i) = -1$ when $M_i - M_{i-1} < 0$. Because $R_i(x) = (|M_i - M_{i-1}|(x - x_i))^+$, for any $x \in [x_k, x_{k+1}]$,

$$\begin{aligned} G(x) &= \sum_{i=0}^{N-1} sgn(i) R_i + f(x_0) \\ &= \sum_{i=0}^{N-1} sgn(i) (|M_i - M_{i-1}|(x - x_i))^+ + f(x_0) \\ &= \sum_{i=0}^{N-1} (M_i - M_{i-1})(x - x_i)^+ + f(x_0) \\ &= \sum_{i=0}^k (M_i - M_{i-1})(x - x_i) + f(x_0) \\ &= \sum_{i=0}^k (M_i - M_{i-1})x - \sum_{i=0}^k (M_i - M_{i-1})x_i + f(x_0) \\ &= M_k x - M_k x_k + \sum_{i=0}^{k-1} M_i (x_{i+1} - x_i) + f(x_0) \\ &= M_k (x - x_k) + \sum_{i=0}^{k-1} (f(x_{i+1}) - f(x_i)) + f(x_0) \\ &= M_k (x - x_k) + f(x_k) \\ &= f_k(x), \end{aligned} \quad (7)$$

which indicates that $G(x)$ can exactly express $f(x)$ in Eq. (2).

To illustrate the idea clearly, we exemplify $\sum_{i=0}^2 \operatorname{sgn}(i)R_i + f(x_0)$ as $R_0 + R_1 - R_2 + f(x_0)$, as shown in Figure 2.

Based on the above derivation, for any $f(x)$ consisting of N piecewise linear segments and the first piece is non-constant, there will be a function $f(x_0) + \sum_{i=0}^{N-1} R_i$ constructed by a one-neuron-wide N -layer network in the proposed topology that can exactly represent $f(x)$. Because $f(x)$ can approximate any continuous univariate function, **Conjecture 1** is verified.

Now, let us analyze the limit of N . Suppose $g \in C^1 : [0, 1] \rightarrow \mathbb{R}$, because $|g(x) - g(y)| \leq \int_{|x-y| \leq \eta} |g'(s)|ds \leq \eta \|g'\|_\infty$, where $\|g'\|_\infty$ is the maximum absolute value of the derivative of g , a continuous piecewise linear function f can represent g in terms of $\sup_x |g - f| < \delta$, as long as we partition $[0, 1]$ into intervals whose lengths are smaller than $\delta/\|g'\|_\infty$. As a result, the required number of pieces is $1/\delta/\|g'\|_\infty = \|g'\|_\infty/\delta$. Because the sparse shortcut network G can represent the piecewise function f directly, the needed neuron number for G is also $N = \|g'\|_\infty/\delta$.

Remark 1: An interesting question is whether the densely connected topology in the DenseNet is necessary or not. Zhu *et al.* [35] experimentally demonstrated that a sparse version of DenseNet has been excellent in image classification, while our **Conjecture 1** theoretically confirms that given the sufficient depth, the densely connected topology has certain redundancy in view of representation ability, since a one-neuron-wide network with the proposed topology can already work for general approximation.

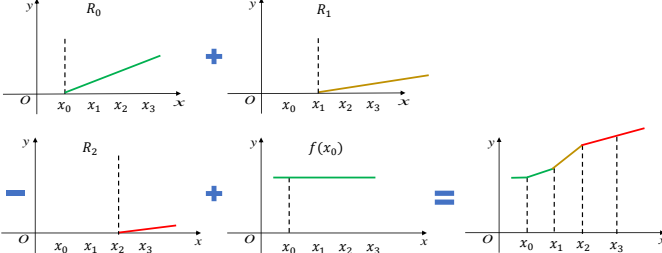


Fig. 2. An example of $\sum_{i=0}^{N-1} \operatorname{sgn}(i)R_i + f(x_0)$ as $R_0 + R_1 - R_2 + f(x_0)$ to illustrate how a one-neuron wide network can represent $f(x)$.

B. Width-bounded universal approximator

Inspired by the feasibility of using a one-neuron-wide network to approximate any continuous univariate function, here we present an alternative width-bounded universal approximator, in analogue to a depth-bounded universal approximator. Width-bounded networks mean that the width of a network is limited but the network can be arbitrarily deep. Our scheme is based on the topology in Figure 1 and the Kolmogorov-Arnold representation theorem. Specifically, we employ the Kolmogorov-Arnold representation theorem to bridge the gap between approximating univariate and multivariate functions.

Conjecture 2: With ReLU activation functions, for any continuous function $f : [0, 1]^n \rightarrow \mathbb{R}$ and any given precision $\sigma > 0$, there exists a neural network W with width no more

than $2n^2 + n$ per layer such that

$$\sup_{x_1, x_2, \dots, x_n \in [0, 1]} |f(x_1, x_2, \dots, x_n) - W(x_1, x_2, \dots, x_n)| < \sigma. \quad (8)$$

Kolmogorov-Arnold representation theorem [25]: According to the Kolmogorov-Arnold representation theorem, for any continuous function $f(x_1, \dots, x_n)$ with $n \geq 2$, there exists a group of continuous functions: $\phi_{q,p}$, $q = 0, 1, \dots, 2n$; $p = 1, 2, \dots, n$ and Φ_q such that

$$f(x_1, x_2, \dots, x_n) = \sum_{q=0}^{2n} \Phi_q \left(\sum_{p=1}^n \phi_{q,p}(x_p) \right). \quad (9)$$

Scheme of analysis: The representation theorem implies that any continuous function $f(x_1, \dots, x_n)$ can be written as a composition of finitely many univariate functions. As shown in Figure 3, our scheme of approximating a multivariate continuous function $f(x_1, \dots, x_n)$ is to first employ $2n^2 + n$ single-neuron-wide network in the proposed topology to represent $\phi_{q,p}(x_p)$ in a parallel manner. Next, suggested by the right side of Eq. (9), we summate the group of functions $\{\phi_{q,1}(x_1), \phi_{q,2}(x_2), \dots, \phi_{q,n}(x_n)\}$ and feed $\sum_{p=1}^n \phi_{q,p}(x_p)$ into a new one-neuron-wide network whose purpose is to approximate Φ_q . Finally, we summate the yields of those $2n + 1$ sub-networks as the ultimate output of the overall network.

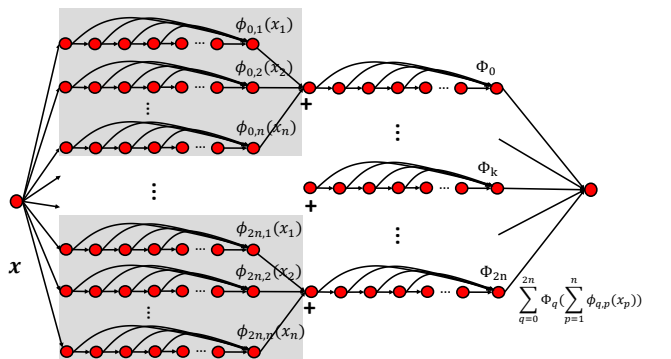


Fig. 3. The scheme of a width-bounded universal approximator.

Analysis: As we have shown in the **Conjecture 1**, for every function $\phi_{q,p}(x_p)$, there exists a function $D_{q,p}(x_p)$ represented by a one-neuron-wide network in the proposed topology such that

$$\sup_{x_p \in [0, 1]} |\phi_{q,p}(x_p) - D_{q,p}(x_p)| < \delta_{q,p}, \quad (10)$$

where $\delta_{q,p} > 0$ is a given arbitrarily small quantity. After we integrate $\{\phi_{q,1}(x_1), \phi_{q,2}(x_2), \dots, \phi_{q,n}(x_n)\}$, for any selection of $x_1, x_2, \dots, x_n \in [0, 1]$, applying triangle inequality, we obtain the error of adding $D_{q,p}$ with respect to p from

Eq. (10):

$$\begin{aligned}
& \sup_{x_1, x_2, \dots, x_n \in [0,1]} \left| \sum_{p=1}^n \phi_{q,p}(x_p) - \sum_{p=1}^n D_{q,p}(x_p) \right| \\
& \leq \sup_{x_1, x_2, \dots, x_n \in [0,1]} \sum_{p=1}^n |\phi_{q,p}(x_p) - D_{q,p}(x_p)| \\
& < \sum_{p=1}^n \delta_{q,p}.
\end{aligned} \tag{11}$$

Given that Φ_q is continuous, we employ the $\epsilon-\delta$ definition of continuity: if $g(x)$ is continuous at x_0 , for any positive number ϵ , there exists $\delta(\epsilon, g) > 0$ satisfying that $|g(x) - g(x_0)| < \epsilon$ when $|x - x_0| < \delta$. Let $\epsilon = \frac{\sigma}{4n+2}$, correspondingly we appropriately choose $\delta_{q,p}$ so that $\sum_{p=1}^n \delta_{q,p} < \delta(\frac{\sigma}{4n+2}, \Phi_q)$. In this case, for every Φ_q , we have the following:

$$\begin{aligned}
& \sup_{x_1, x_2, \dots, x_n \in [0,1]} \left| \Phi_q \left(\sum_{p=1}^n \phi_{q,p}(x_p) \right) - \Phi_q \left(\sum_{p=1}^n D_{q,p}(x_p) \right) \right| \\
& < \frac{\sigma}{4n+2}.
\end{aligned} \tag{12}$$

Every continuous function Φ_q is supported on \mathbb{R} instead of $[0, 1]$. Without loss of generality, we can still find a one-neuron-wide network in the proposed topology to approximate Φ_q arbitrarily well. Let $D_q(x)$ be the function expressed by such a network that can approximate Φ_q in the precision of $\frac{\sigma}{4n+2}$, we have

$$\sup_{x \in \mathbb{R}} |\Phi_q(x) - D_q(x)| < \frac{\sigma}{4n+2}. \tag{13}$$

The above equation means that $D_q(x)$ can represent $\Phi_q(x)$ with an error no greater than $\frac{\sigma}{4n+2}$ over \mathbb{R} . Introducing an intermediate term $\Phi_q(\sum_{p=1}^n D_{q,p}(x_p))$ and applying the triangle inequality to estimate the error of feeding the summation of $D_{q,p}$ into D_q , we have

$$\begin{aligned}
& \sup_{x_1, x_2, \dots, x_n \in [0,1]} \left| \Phi_q \left(\sum_{p=1}^n \phi_{q,p}(x_p) \right) - D_q \left(\sum_{p=1}^n D_{q,p}(x_p) \right) \right| \\
& = \sup_{x_1, x_2, \dots, x_n \in [0,1]} \left| \Phi_q \left(\sum_{p=1}^n \phi_{q,p}(x_p) \right) - \Phi_q \left(\sum_{p=1}^n D_{q,p}(x_p) \right) \right. \\
& \quad \left. + \Phi_q \left(\sum_{p=1}^n D_{q,p}(x_p) \right) - D_q \left(\sum_{p=1}^n D_{q,p}(x_p) \right) \right| \\
& \leq \sup_{x_1, x_2, \dots, x_n \in [0,1]} \left| \Phi_q \left(\sum_{p=1}^n \phi_{q,p}(x_p) \right) - \Phi_q \left(\sum_{p=1}^n D_{q,p}(x_p) \right) \right| \\
& \quad + \sup_{x_1, x_2, \dots, x_n \in [0,1]} \left| \Phi_q \left(\sum_{p=1}^n D_{q,p}(x_p) \right) - D_q \left(\sum_{p=1}^n D_{q,p}(x_p) \right) \right| \\
& < \frac{\sigma}{4n+2} + \frac{\sigma}{4n+2} = \frac{\sigma}{2n+1},
\end{aligned} \tag{14}$$

where we enforce Eqs. (12) and (13) to derive from the second and third lines to the fourth line. Then, applying the triangle inequality for the summation of D_q , $q = 0, \dots, 2n$, we immediately obtain the error of the total approximation

scheme of Kolmogorov-Arnold representation theorem from Eq. (9):

$$\begin{aligned}
& \sup_{x_1, x_2, \dots, x_n \in [0,1]} \left| \sum_{q=0}^{2n} \Phi_q \left(\sum_{p=1}^n \phi_{q,p}(x_p) \right) - \sum_{q=0}^{2n} D_q \left(\sum_{p=1}^n D_{q,p}(x_p) \right) \right| \\
& \leq \sup_{x_1, x_2, \dots, x_n \in [0,1]} \sum_{q=0}^{2n} \left| \Phi_q \left(\sum_{p=1}^n \phi_{q,p}(x_p) \right) - D_q \left(\sum_{p=1}^n D_{q,p}(x_p) \right) \right| \\
& < (2n+1) \times \frac{\sigma}{2n+1} = \sigma.
\end{aligned} \tag{15}$$

Let $W(x_1, x_2, \dots, x_n) = \sum_{q=0}^{2n} D_q \left(\sum_{p=1}^n D_{q,p}(x_p) \right)$, we immediately get the validity of **Conjecture 2**.

Remark 2: Here, we present a novel width-limited universal approximator with the width no more than $2n^2 + n$ per layer. This width bound is greater than those of other width-bounded universal approximators: $n+4$ in [26] and $n+1$ in [28]. In addition, this bound is greater than the architectures of the state-of-the-art models, even comparing with the wide residual networks (WRN) on CIFAR10, where the bound is $2 \times 1024^2 + 1024$ and the width of the employed network is 192. Despite that the width bound here is not practical, due to the scarcity of width-bounded universal approximators and the novelty of our construction, it is still a valuable addition to the existing work. In addition, Kolmogorov-Arnold representation theorem was revisited in [36]. The smoothness property of interior functions $\phi_{q,p}$ of the Kolmogorov-Arnold representation was enhanced by modifying the interior functions as a mapping from digits of a binary expansion to digits of a ternary expansion. Such a modification enables a ReLU network to realize the modified Kolmogorov-Arnold representation. However, the resultant network has $2K+3$ layers with $\{n, 4n, \dots, 4n, n, 1, 2^{Kn}+1, 1\}$ neurons at each layer respectively, where K is a positive number up to the pre-specified approximation precision. Such a network is neither depth-bounded nor width-bounded.

C. A family of networks

Motivated by our constructive proof for the proposed topology, we report that in the one-dimensional setting, the aforementioned analysis is translatable to a rather inclusive family of network topologies. This network family (denoted as Ω^M) subsumes an extremely wide network, an extremely deep network, and networks between them, where M is the number of hidden neurons, not including the input node and output node. We argue that network topologies in Ω^M are equivalent in the sense of their approximation ability. Furthermore, we present the spectral characterization for Ω^M .

The input node is also considered as the neuron for simplicity. Hence, we refer neurons as three types: hidden neurons, the input neuron, and the output neuron. A network in Ω^M shall satisfy the following three conditions:

- 1) Every hidden neuron has one inbound edge.
- 2) Every hidden neuron and the input neuron have one outbound edge that links to the output neuron.

3) The input neuron is wired with at least one hidden neuron.

Apparently, the first condition can be trivially relaxed to that every hidden neuron has multiple inbound edges by setting weights of extra shortcuts as zero. The examples that belong to Ω^6 are shown in Figure 4. For a topology in Ω^M , the number of required edges should be $2M + 1$. One thing worthwhile to highlight is that members in Ω^M are mutually convertible through one or more cutting-rewiring operations. A cutting-rewiring operation means that cutting the current input edge of one neuron and rewiring the one with some other neuron. Regarding the network belonging to a network family Ω , we have the following conjecture:

Conjecture 3: With ReLU activation functions, for any continuous function $g : [0, 1] \rightarrow \mathbb{R}$ and any given precision $\delta > 0$, there is a network family Ω^N in which any network K , whose mapping is denoted as $\Omega_K^N(x)$, satisfies:

$$\sup_{x \in [0, 1]} |g(x) - \Omega_K^N(x)| < \delta. \quad (16)$$

The sketch of analysis: Similarly, the core of the problem is how to represent a continuous piecewise function $f(x)$ of N pieces by a network from $\Omega^N(x)$. The main difference is that the hidden neuron in a network from $\Omega^N(x)$ is allowed to get the information from any previous neurons other than just exactly from the previous neighboring neuron.

Analysis: For convenience and without loss of generality, we still use $f(x)$ in Eq. (2). To arrive **Conjecture 3**, we need to use $\Omega_K^N(x)$ to express $f(x)$.

Now we show how weights and bias in each neuron are appropriately selected in $\Omega_K^N(x)$ to approximate $f(x)$. Without loss of generality, the neurons are denoted as $Q_{input}, Q_0, \dots, Q_{N-1}, Q_{output}$, where Q_{input} is the input node, Q_0 is connected to the input neuron directly and Q_{i+1} is fed with either the input neuron or some neuron $Q_t, t \leq i$, and Q_{output} is the output neuron. Accordingly, the outputs of neurons Q_0, Q_1, \dots, Q_{N-1} are also denoted as Q_0, Q_1, \dots, Q_{N-1} for convenience, and our goal is to let Q_0, Q_1, \dots, Q_{N-1} to represent $f_0, f_1, f_2, \dots, f_{N-1}$ at $[x_0, x_1], (x_1, x_2], \dots, (x_{N-1}, x_N]$ without a constant shift respectively.

For Q_0 , similar to what we did before, we set that

$$Q_0 = (|M_0| (x - x_0))^+. \quad (17)$$

For Q_{i+1} , suppose that it connects with Q_j , we set that

$$Q_{i+1} = \left(|M_{i+1} - M_i| \times \left(\frac{1}{|M_j - M_{j-1}|} Q_j - x_{i+1} + x_j \right) \right)^+. \quad (18)$$

Thus, the output of each neuron fulfills $Q_i(x) = (|M_i - M_{i-1}|(x - x_i))^+$. Similarly, we aggregate the output of all N hidden neurons in the output neuron as

$$\Omega_K^N(x) = \sum_{i=0}^{N-1} \text{sgn}(i) Q_i + f(x_0), \quad (19)$$

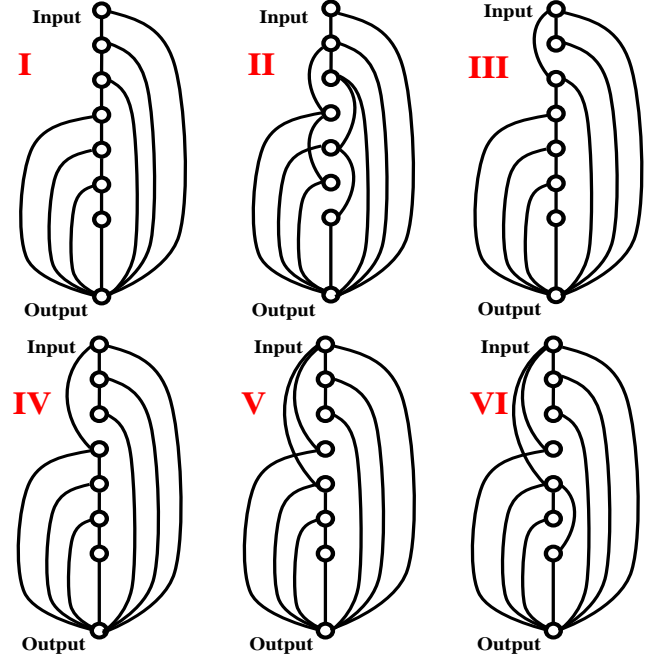


Fig. 4. Six exemplary structures in Ω^8 combined with ResNet setup are used to test if the networks in Ω are truly equivalent or not.

which is equal to $f(x)$ according to Eq. (7). Therefore, we arrive **Conjecture 3**.

Remark 3: Our representation ability analysis suggests that the members of Ω are equivalently expressive. We would like to emphasize that such a finding is important in both theoretical and practical senses. On the one hand, both a one-hidden-layer but super wide network and a one-neuron-wide but super deep network are demonstrated to have strong expressive ability. A natural curiosity is what about the networks in between. Are they also permitting a good approximation ability? Here, we partially answer this question in the one-dimensional setting since the network family Ω comprises of a wide network, a deep network, and networks in between. They are equally capable in terms of approximating a univariate function. On the other hand, network design is an important research direction. Changing where to take inputs makes no impact on the approximation ability of the network, by which the insight can be drawn to network architecture design and search [13]. Since we discovered that a good amount of networks are actually equivalent to each other, the search and design cost will be much reduced in principle considering the shortcut topology is essential in neural architecture search and design.

IV. GENERALIZATION BOUND ANALYSIS

As mentioned earlier, for a shortcut topology, there are two types of aggregations for shortcuts: summation (+) and concatenation (\oplus). The effect of summation connections on the generalizability of deep networks has been studied in [31]. To fill the gap that the concatenation shortcuts are not explored, in this section, we dissect the generalizability of concatenation shortcuts by computing the generalization bounds from theories. A generalization bound, which quanti-

tatively expresses the generalization ability of a model, is the upper bound of the generalization error. Recently, aimed at explaining good generalizability of over-parameterized deep networks, a plethora of norm-based generalization bounds [37]–[39] that rely on weight matrices norms rather than the number of weights are developed. These bounds make sense in explanation because they eliminate direct dependence on the number of parameters.

Here, we derive the norm-based generalization bounds of DenseNet, with an emphasis on the spectrally normalized margin-based generalization bound [37]. To the best of our knowledge, our study is the first to analyze the effect of concatenation shortcuts on the generalization ability of deep networks. Then, we show that the generalization bound of the network using the proposed topology is tighter than that of the DenseNet, which suggests that the proposed topology can generalize well.

First, the data norm is set to the l_2 norm and the operator norm set to the spectral norm $\|\cdot\|_\sigma$, where $\|\cdot\|_\sigma$ is defined as $\|A\|_\sigma = \sup_{\|Z\|_2 \leq 1} \|AZ\|_2$. Furthermore, $\|\cdot\|_{p,q}$ is the matrix (p,q) -norm defined as $\|A\|_{p,q} = \|(\|A_{:,1}\|_p, \dots, \|A_{:,m_2}\|_p)\|_q$ for $A \in \mathbb{R}^{N \times m_2}$. $\ln(\cdot)$ is the natural logarithm.

Next, we denote the model as $F(\mathbf{x})$ and define the margin operator $\mathcal{M} : \mathbb{R}^k \times \{1, 2, \dots, k\} \rightarrow \mathbb{R}$ for the k -class classification task as $F(\mathbf{x})_z - \max_{j \neq z} F(\mathbf{x})_j$ for the z^{th} ground truth class, where z is the class index, and the ramp function is

$$l_\gamma(r) = \begin{cases} 0 & r < -\gamma \\ 1 + r/\gamma & -\gamma \leq r \leq 0 \\ 1 & r > 0, \end{cases} \quad (20)$$

where γ is the margin controlling the slope of $l_\gamma(r)$. Then, the empirical ramp loss over the dataset $D = \{(\mathbf{x}_1, y_1), \dots, (\mathbf{x}_n, y_n)\}$ is

$$\hat{\mathcal{R}}_\gamma(F) = \frac{1}{n} \sum_{i=1}^n (l_\gamma(-\mathcal{M}(F(\mathbf{x}_i), y_i))). \quad (21)$$

Minimizing the empirical ramp loss is equivalent to maximizing the margin of the predicted classes in the dataset. With all the notations and definitions, we have the following theorem.

Theorem 1: Let us fix nonlinear activation functions $\sigma_1, \dots, \sigma_L$, where σ_i is ρ_i -Lipschitz and $\sigma_i(0) = 0$. Furthermore, let the margin $\gamma > 0$, spectral norm bounds (s_1, \dots, s_L) , data bound B , and matrices $(2, 1)$ -norm bounds (b_1, \dots, b_L) be given. Then, with at least $1 - \delta$ probability over N samples $((\mathbf{x}_i, y_i)_{i=1}^N)$ with $\mathbf{x}_i \in \mathbb{R}^d$, $\sqrt{\sum_i \|\mathbf{x}_i\|_2^2} \leq B$ are drawn from identical and independent distribution, every DenseNet in $F_A : \mathbb{R}^d \rightarrow \mathbb{R}^k$ defined

as

$$\left\{ \begin{array}{l} G_0 = X^T \\ F_1 = A_1 X^T \\ G_i = \sigma_i(F_i) \\ F_{i+1} = A_{i+1} \oplus_{k=0}^i G_k \\ F_L = A_L \oplus_{k=0}^{L-1} G_k, \end{array} \right. \quad (22)$$

where $X \in \mathbb{R}^{N \times d}$ collects data samples $\{\mathbf{x}_i\}_{i=1}^N$, \oplus is the matrix concatenation along the row direction, $\oplus_{k=0}^i G_k = G_1 \oplus G_2 \dots \oplus G_k = [G_0; G_1; \dots; G_k]$, A_i is of $d_i \times n_i$ with $n_i = \sum_{k=0}^{i-1} d_k$, the matrices $\mathcal{A} = (A_1, \dots, A_L)$ with $A_i \in \mathbb{R}^{d_i \times n_i}$, $n_i = \sum_{k=0}^{i-1} d_k$ obey that $\|A_i\|_\sigma \leq s_i$ and $\|A_i^T\|_{2,1} \leq b_i$, and L is the number of layers, satisfies

$$\begin{aligned} & \Pr\{\arg \max_i F_A(\mathbf{x})_i \neq y\} - \hat{\mathcal{R}}_\gamma(F_A) \\ & \leq \frac{8}{n^{3/2}} + 3\sqrt{\frac{\ln(1/\delta)}{2n}} + \\ & \frac{36B\ln(n)\prod_{i=1}^L(1+\rho_i s_i)}{\gamma n} \sqrt{\sum_{i=1}^L \frac{\rho_i^2 b_i^2}{(1+\rho_i s_i)^2} \ln(2d_i n_i)}. \end{aligned} \quad (23)$$

For conciseness, we put its proof in the **Theorem 1** of Part A of supplementary materials.

Remark 4: Please note that our result is based on the proof in [37], and is the first to apply the results on the chain-like networks into the networks with concatenation shortcuts to evaluate the impact of concatenation shortcuts on the generalization bound of deep networks. As shown in Table I, we compare the bounds of the DenseNet and chain-like network. The incorporation of dense concatenation shortcuts leads to a higher generalization bound than the chain-like network due to the increased matrix size $n_i = \sum_{k=0}^{i-1} d_k > d_{\max}$. However, the bounds of the DenseNet and chain-like network are close when small weight matrices are used in each layer. This result partially explains why the DenseNet performs well in a small filter size because in this situation, the concatenation shortcuts only moderately elevate the generalization bound.

TABLE I
THE GENERALIZATION BOUNDS FOR THE DENSENET AND CHAIN-LIKE NETWORK. d_{\max} IS THE MAXIMUM WIDTH.

Models	Generalization Bound
DenseNet	$\mathcal{O}\left(\prod_{i=1}^L(1+\rho_i s_i)\sqrt{\sum_{i=1}^L \frac{\rho_i^2 b_i^2}{(1+\rho_i s_i)^2} \ln(2d_i n_i)}\right)$
Chain-like	$\mathcal{O}\left(\prod_{i=1}^L(\rho_i s_i)\sqrt{\sum_{i=1}^L \frac{b_i^2}{s_i^2} \ln(2d_{\max}^2)}\right)$

What's more, we apply the techniques from [38] which derived a generalization bound by directly estimating Rademacher complexity into the DenseNet, and the resultant bound is summarized in Table II. The proof is put into Part B of supplementary materials. From Table II, we can show that the Rademacher-based generalization bound of the DenseNet is also close to that of the chain-like network.

TABLE II

THE GENERALIZATION BOUNDS FOR DENSENET BY THE APPROACH OF [38]. $B_{i,F}$ DENOTES THE UPPER BOUNDS OF FROBENIUS NORM OF THE WEIGHT MATRIX IN THE i^{th} LAYER. m IS THE SIZE OF DATA.

Models	Generalization Bound
DenseNet	$\mathcal{O}\left(\frac{\prod_{i=1}^L(1+2B_{i,F})}{\sqrt{m}}\right)$
Chain-like	$\mathcal{O}\left(\frac{2^L \cdot \prod_{i=1}^L B_{i,F}}{\sqrt{m}}\right)$

Conjecture 4: The margin-based multi-class generalization bound of the network in the proposed topology is tighter than that of the DenseNet.

Insight: The core part of the derived bound in Eq. (23) is the third term of the right side, which is mainly dependent upon the spectral norm bound s_i and the matrix (2, 1)-norm bound b_i of weight matrices. Because by adding imaginary shortcuts but setting the extra weight matrices as zeros, the proposed topology becomes a special case of the DenseNet, the spectral norm bounds and matrix (2, 1)-norm bounds of the proposed topology are no more than those of the DenseNet. As a consequence, the spectrally normalized margin-based generalization bound of the network in the proposed topology is tighter than that of the DenseNet.

Analysis: Let us derive the margin-based multi-class generalization bound of the network in the proposed topology and compare it with that of the DenseNet. To discriminate them, in the following we use the superscript (S) for the parameters pertaining to the former and the superscript (D) to denote the parameters pertaining to the latter. Then, Eq. (23) turns into

$$\begin{aligned} & \Pr\{\arg \max_i F_{\mathcal{A}}^{(D)}(\mathbf{x})_i \neq y\} - \hat{\mathcal{R}}_{\gamma}(F_{\mathcal{A}}^{(D)}) \\ & \leq \frac{8}{n^{3/2}} + 3\sqrt{\frac{\ln(1/\delta)}{2n}} + \\ & \frac{36B\ln(n) \prod_{i=1}^L (1 + \rho_i s_i^{(S)})}{\gamma n} \sqrt{\sum_{i=1}^L \frac{\rho_i^2 b_i^{(D)2}}{(1 + \rho_i s_i^{(D)})^2} \ln(2d_i n_i^{(D)})}. \end{aligned} \quad (24)$$

For a fair comparison, we set the output dimension of each layer in the network of the proposed topology to the same as that of the DenseNet. Also, we use d_i for both networks. Let $A_i^{(S)}$ be of $d_i \times n_i^{(S)}$, where $n_i^{(S)} = d_{i-1}$, $i \leq L-1$, $n_L^{(S)} = \sum_{i=1}^{L-1} d_i$ and $X \in \mathbb{R}^{n \times d}$. The computational structure of the network of the proposed topology is

$$\left\{ \begin{array}{l} G_0^{(S)} = X^T \\ F_1^{(S)} = A_1^{(S)} X^T \\ G_i^{(S)} = \sigma_i(F_i^{(S)}) \\ F_{i+1}^{(S)} = A_{i+1}^{(S)} G_i^{(S)}, i \leq L-2 \\ F_L^{(S)} = A_L^{(S)} \oplus_{k=0}^{L-1} G_k^{(S)}. \end{array} \right. \quad (25)$$

Without changing the final output, we can rewrite the above structure by adding imaginary shortcuts and setting the extra weight matrices as zeros, without changing the function of the model,

$$\left\{ \begin{array}{l} G_0^{(S)} = X^T \\ F_1^{(S)} = A_1^{(S)} X^T \\ G_i^{(S)} = \sigma_i(F_i^{(S)}) \\ F_{i+1}^{(S)} = [A_{i+1}^{(S)}, \mathbf{0}^{d_{i+1} \times \sum_{k=0}^i d_k}] [G_i^{(S)}; \mathbf{0}^{d_i \times n}; \dots; \mathbf{0}^{d_0 \times n}] \\ F_L^{(S)} = A_L^{(S)} \oplus_{k=0}^{L-1} G_k^{(S)}, \end{array} \right. \quad (26)$$

where $\mathbf{0}^{C_1 \times C_2}$ means the zero matrix of $C_1 \times C_2$. The network in the proposed topology is a special DenseNet with specific weight matrices as zeros. We can estimate the generalization bound for the above zero-padded network Eq. (26) by mimicking the generalization bound of DenseNet:

$$\begin{aligned} & \Pr\{\arg \max_i F_{\mathcal{A}}^{(S)}(\mathbf{x})_i \neq y\} - \hat{\mathcal{R}}_{\gamma}(F_{\mathcal{A}}^{(S)}) \\ & \leq \frac{8}{n^{3/2}} + 3\sqrt{\frac{\ln(1/\delta)}{2n}} + \\ & \frac{36B\ln(n) \prod_{i=1}^L (1 + \rho_i s_i^{(S)})}{\gamma n} \sqrt{\sum_{i=1}^L \frac{\rho_i^2 b_i^{(S)2}}{(1 + \rho_i s_i^{(S)})^2} \ln(2d_i n_i^{(D)})}, \end{aligned} \quad (27)$$

where $n_i^{(D)}$ is used because the matrix size has been enlarged to the same to that of the DenseNet.

To verify **Conjecture 4**, we need to compare the bounds of DenseNet and the proposed topology (Eq. (24) vs Eq. (27)). According to the definition of the spectral norm, we have

$$\begin{aligned} & \|A_i^{(S)}\|_{\sigma} \\ & = \sup_{\|Z\|_2 \leq 1} \|A_i^{(S)} Z^{(S)}\|_2 \\ & = \sup_{\|Z\|_2 \leq 1} \|[A_i^{(S)}, \mathbf{0}^{d_i \times (n_i^{(D)} - n_i^{(S)})}] \|[Z; \mathbf{0}^{(n_i^{(D)} - n_i^{(S)}) \times n}]\|_2 \\ & \leq \sup_{\|Z\|_2 \leq 1} \|A_i^{(D)} Z^{(D)}\|_2 \\ & = \|A_i^{(D)}\|_{\sigma}, \end{aligned} \quad (28)$$

where zero padding is to make $[A_i^{(S)}, \mathbf{0}]$ have the same size as that of $A_i^{(D)}$. Therefore, we derive that

$$s_i^{(S)} \leq s_i^{(D)}, i = 1, \dots, L. \quad (29)$$

In the same spirit, we can also derive that

$$b_i^{(S)} \leq b_i^{(D)}, i = 1, \dots, L. \quad (30)$$

Combining Eqs. (29) and (30), we have

$$\begin{aligned} & \prod_{i=1}^L (1 + \rho_i s_i^{(S)}) \sqrt{\sum_{i=1}^L \frac{\rho_i^2 b_i^{(S)2}}{(1 + \rho_i s_i^{(S)})^2} \ln(2d_i n_i^{(D)})} \leq \\ & \prod_{i=1}^L (1 + \rho_i s_i^{(D)}) \sqrt{\sum_{i=1}^L \frac{\rho_i^2 b_i^{(D)2}}{(1 + \rho_i s_i^{(D)})^2} \ln(2d_i n_i^{(D)})}, \end{aligned} \quad (31)$$

which has validated **Conjecture 4**.

Remark 5: Our representation and generalization analyses suggest that DenseNet has certain redundancy in terms of representation ability, and it has higher generalization bound based on generalization bound analysis. However, the redundant structure of DenseNet may facilitate over-parameterization effect. Recently, extensive research has shown that redundant networks enjoy considerable merits in optimization and generalization due to the over-parameterization effect. For instance, regarding merits in optimization, stochastic gradient descent (SGD) is able to find the global minimum in shallow or deep networks in the setting of over-parameterization, there is a large set of global minima in an overly parameterized network [40]–[42]. Over-parameterization is also beneficial for generalization [43], [44]. Recently, deep double descent, which describes a phenomenon that when the model complexity increases, the generalization error goes down first and then goes up. However, as the model complexity keeps increasing and surpasses a so-called "interpolation threshold", the generalization error starts going down, has been widely observed in many deep models [44]. In light of the double descent phenomenon, it is likely that the complexity of DenseNet lies beyond the interpolation threshold.

V. EXPERIMENT

In this section, we conduct prediction and classification experiments on well-known benchmarks to evaluate the expressibility and generalizability of the proposed topology. The expressive experiments use summation (+) shortcuts, while the generalizability and interpretability experiments use concatenation (\oplus) shortcuts. The competitive performance on prediction and classification tasks shows that the proposed topology is a desirable architecture, as suggested by encouraging theoretical analyses. In addition, we also show the superior interpretability of the investigated topology in view of layer importance and saliency map.

A. Expressibility

We compare the expressibility of the proposed topology and residual topology in the infinite-width limit, where the gradient descent makes little change to the weights of a network. Therefore, the training of a neural network with infinite width in each layer turns into a kernel ridge regression [45] process with the so-called neural tangent kernel (NTK) [46]. When one fixes the form of activation functions, the neural tangent kernel of a neural network is only determined by the topology and the depth of the network [47]. Figure 5 shows the structures of the proposed network and a residual network which uses pre-activation features. In the proposed network, the output of each dense layer is connected to a layer before the final dense layer for summation. We denote the depth of two networks as $K + 2$, where K is the number of residual blocks or the number of layers that constitute the proposed topology. The two networks are the same except the shortcut architectures. Let samples of training dataset be $\{(x_i, y_i)\}_{i=1}^n$, where x_i is the input and y_i is the ground-truth output, and assume that $f(\theta, x)$ denotes the output of

a neural network, where θ are the weights and biases, the (i, j) -entry of the NTK kernel \mathbf{H}^* [47] is defined by

$$\text{ker}(x_i, x_j) = \mathbb{E}_{\theta \sim \Theta} \left\langle \frac{\partial f(\theta, x_i)}{\partial \theta}, \frac{\partial f(\theta, x_j)}{\partial \theta} \right\rangle. \quad (32)$$

The inference is deterministic:

$$f(\mathbf{x}) = [\text{ker}(\mathbf{x}, \mathbf{x}_1), \dots, \text{ker}(\mathbf{x}, \mathbf{x}_n)] \cdot (\mathbf{H}^*)^{-1} \mathbf{y} \quad (33)$$

We argue that the comparison in the NTK domain can avoid the effect of other model hyper-parameters such as ways of training and so on. This can help reveal the true representation ability of two topologies, since the inference of kernel ridge regression is deterministic, and the kernel is only decided by the topology and the depth.

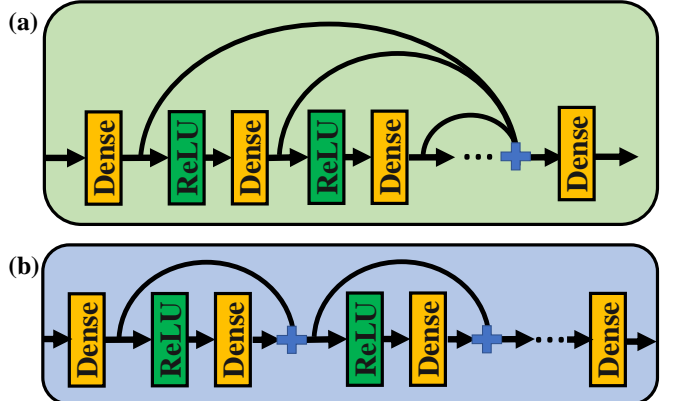


Fig. 5. "Dense" denotes a fully connected layer. (a) The network of the proposed topology; (b) the network of residual topology.

We use the Boston house prices dataset [48] as a test bed that has 13 attributes including average number of rooms, pupil-teacher ratio, and so on as the input. The task is to predict the house price based on the attributes of a house. The dataset is randomly split into a training set (90%) and a test set (10%). The mean squared error between predictions and ground-truth is computed as the evaluation metric. We vary K from 4 to 10 to make a thorough comparison. The code is written online in Google Colab based on Python neural tangent package (<https://github.com/google/neural-tangents>). For all K , the inference time is no more than 10 seconds. Figure 6 highlights the consistent improvement of the proposed topology over the residual one. In addition, while the mean squared errors of both models keep going down as K increases, the downward momentum of the proposed topology is stronger.

B. Generalizability

Here, we validate the generalizability of the proposed topology with concatenations to see if it can truly deliver competitive results as promised. Suppose that y_l is the output of the l^{th} module in the network of L layers, we characterize the workflow of the proposed topology in the following way:

$$\begin{aligned} y_{l+1} &= H_l(y_l), \\ y_L &= H_{L-1}(y_0 \oplus y_1 \oplus y_2 \oplus \dots \oplus y_{L-1}), \end{aligned} \quad (34)$$

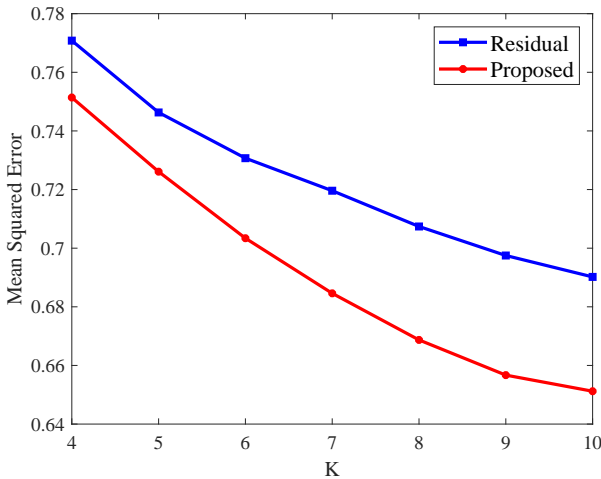


Fig. 6. Results of NTK kernel ridge regression of the residual topology and the proposed topology on the Boston house prices dataset.

where \oplus is a concatenation operator. The operator module $H(\cdot)$ can perform multiple operations including batch normalization [49], convolution, dropout [50], and so on. While the multiplication operation is the mainstay in our theoretical analysis, the theory also works for the convolution operation for the following reasons. On one hand, our analysis highlights the utility of the structure. On the other hand, the convolution operation is a kind of multiplication because the convolution between two vectors can be re-formulated as a matrix multiplication. In this regard, the generalizability analysis based on multiplication operations is also effective.

The network of the proposed topology is implemented as a drop-in replacement for the DenseNet, which means that the only difference between our network and DenseNet is the shortcut topology. Our model comprises of multiple blocks, and each block employs the proposed topology. The important hyperparameters for our model are also the feature growth rate k and the number of layers in each block that determines the depth. The number of features of a layer is referred as the growth rate, and it regulates how much information is passed to the final state. We compare the proposed topology with other advanced deep learning benchmark models on CIFAR100, Tiny ImageNet, and ImageNet datasets.

CIFAR-100: We follow the initialization strategy in DenseNet. The DenseNet utilizes stage training, where the number of filters across the stages are doubled and the size of feature maps are reduced at the scale of 2. The proposed network includes four blocks. All the model configurations for the proposed model follow the protocol in [12]. The total epoch is 250. The initial learning rate is 0.1 and divided by 10 in every quarter of total epoch number. We use SGD for training with a weight decay of 0.0001 and a momentum of 0.9. We run each of the proposed models five times and computed the corresponding mean and variance of errors. In Table III, we summarize the experimental results on the CIFAR-100. It is seen that the network of the

proposed topology achieves an error rate of 23.52%, which is slightly higher than DenseNet($k=24$, depth=100). It is noted that the proposed model works better at larger growth rates, which is quite different from the DenseNet. Because of the memory constraint, larger growth rates can be prohibitive for the DenseNet. Overall, the proposed topology achieves competitive results over CIFAR-100.

TABLE III
COMPARISONS OF CLASSIFICATION PERFORMANCE ON CIFAR-100
AMONG THE PROPOSED MODEL AND OTHER MODELS.

Network	Params	Error(%)
NIN + Dropout [9]	-	35.68
FractalNet with Dropout [17]	38.6M	35.34
ResNet (Stochastic Depth) [51]	1.7M	37.80
DIANet [52]	-	23.02
SpinalNet [53]	-	35.01
LP-BNN [54]	-	23.02
DenseNet (k=12, depth=40)	1.0M	27.55
DenseNet (k=12, depth=100)	7.0M	23.79
DenseNet (k=24, depth=100)	27.2M	23.42
Proposed (k=12, depth=40)	0.4M	29.63 ± 0.017
Proposed (k=24, depth=40)	1.3M	26.21 ± 0.025
Proposed (k=40, depth=40)	3.6M	23.52 ± 0.037

The errors of compared models are reported by the official implementation.

TABLE IV
COMPARISONS OF CLASSIFICATION PERFORMANCE AMONG VARIOUS
ADVANCING MODELS ON TINY IMAGENET.

Network	I.r.	Params	Error(%)
MobileNetV2 (2018) [55]	0.1	3.5M	43.76
EfficientNet-B0 (2019) [56]	0.1	5.3M	42.91
OctResNet50 (2019) [57]	0.1	25.5M	47.45
Lambda Network (2020) [58]	0.1	15.0M	58.71
SE-Net (2018) [59]	0.05	28.1M	53.98
Scale-Net (2019) [60]	0.01	31.4M	48.59
Ghost-Net (2020) [61]	0.1	5.2M	44.01
RandomWire-WS (2019) [62]	0.01	31.6M	42.11
Proposed A (k=96, depth=41)	0.1	5.0M	42.82 ± 0.31
Proposed B (k=108, depth=41)	0.1	10.6M	42.04 ± 0.24

All models are implemented by us.

Tiny ImageNet dataset: This dataset consists of 200 classes with 500 training, 50 validation, and 50 test images in each class. The images are of 64×64 , which are down sampled from the full images of ImageNet. In the experiments, we select the following models for comparison: MobileNetV2 [55], EfficientNet-B0 [56], OctResNet50 [57], Lambda Network [58], SE-Net [59], Scale-Net [60], Ghost-Net [61], and Randomly Wired Network [62]. All these models are well-known new benchmarks. We set batch size as 64. For choosing the learning rate, we adopt the standard learning rate decay approach. In every 30 epochs, the learning rate is divided by 10. The initial learning rate set to be chosen is $\{0.01, 0.05, 0.1\}$. The momentum is 0.9. All models are trained in two TITAN Xp and one GeForce GTX 1080 GPUs. For all models, maximally, it takes 742.43 seconds to finish one epoch. Based on our tuning, the appropriate hyperparameters for the counterpart models are shown in Table IV. We verify two models ($k=96$, depth=41, init-nf=32) and ($k=96$, depth=41, init-nf=32), where each model

consists of three blocks and "init-nf" means the number of features in the first layer of each block. We run the proposed two models five times and computed the corresponding mean and variance of errors. Table IV shows top-1 validation errors of all models, where both two proposed models achieve state-of-the-art performance. Particularly, the proposed model ($k=108$, depth=41) obtains the lowest error among all models, which indicates again that the proposed model works better with a high growth rate. One thing worthwhile to mention is that the network with the proposed topology is better than the randomly wired network, which demonstrates that the mathematical analysis makes more sense in network design.

ImageNet dataset: The ImageNet dataset [63] consists of 1.2 million images for training, and 50,000 images for validation, which are from 1,000 classes. We follow the data augmentation scheme of [11] for training images. For model configurations, we follow those of DenseNet [12]. We set the batch size as 156, the initial learning rate as 0.1, the weight decay as 0.0001, and the momentum as 0.9. In validation, we adopt the standard 10-crop validation. To be fair, we compare our model with other state-of-the-art models in the small size regime ($< 10M$ parameters) and regular size regime ($\sim 20M$ parameters), respectively. Our models are trained on four GeForce GTX 1080 GPUs. It takes the smaller model around 75 mins per epoch, while it takes the bigger model around 90 mins per epoch. We run the larger model three times and smaller model five times, and we compute the average and variance of errors. Due to the computational burden of searching, NAS-based models appear in the small model regime. Tables V and VI highlight the state-of-the-art results achieved by the proposed model. Regarding the small size regime, in spite of the moderately higher model complexity, the proposed model achieves the lowest error compared to other advanced models. Additionally, considering that our model is free of computationally expensive search, the accuracy achieved by our model is competitive. While for regular model regime, our model is comparable to other advanced models.

C. Interpretability

Interpretability is an essential problem for the development of deep learning [75] and [76]. Here, we also show the superior interpretability of the proposed model in terms of the saliency map.

Saliency map: Currently, saliency methods, which derive a saliency map by identifying relevance between features and the prediction of a model, remain the mainstream of interpretability methods [77]. A myriad of saliency methods are based on gradients [75], the idea of which is that the strength of gradients can mirror how a feature can affect a model output. As we know, shortcuts can facilitate training by alleviating gradient explosion and vanishing. The mechanism is that shortcuts provide additional paths that enable a more accurate and easier gradient propagation as they avoid multiplying gradients many times. We argue that such a mechanism should also be helpful to improve the quality

TABLE V
PERFORMANCE COMPARISONS IN SMALL MODEL REGIME ON
IMAGENET VALIDATION SET.

Network	params	Error(%)
DenseNet121 (2017) [12]	8.0M	25.4
MobileNetV2 (2018) [55]	6.9M	25.3
ShuffleNet (2018) [64]	5.4M	26.3
NASNet-B (2018) [65]	5.3M	27.2
NASNet-C (2018) [65]	4.9M	27.5
Amoeba-A (2018) [66]	5.1M	25.5
Amoeba-B (2018) [66]	5.3M	26.0
PNAS (2018) [67]	5.1M	25.8
DARTS (2019) [68]	4.9M	26.9
FBNet-A (2019) [69]	4.3M	27.0
RandWire-WS (2019) [62]	5.6M	25.3
Proxyless-R (2019)	4.0M	25.4
RegNetX-600MF (2020) [70]	6.2M	25.9
DeiT-Ti (2020)	5.0M	25.4
Proposed (k=96, depth=45)	9.4M	25.2 ± 0.07

The errors of compared models are reported by the official implementation.

TABLE VI
PERFORMANCE COMPARISONS IN REGULAR MODEL REGIME ON
IMAGENET VALIDATION SET.

Network	params	Error(%)
ResNet-50(2016)	21.0M	23.8
ResNet50-B (2018)	25.0M	23.4
SENet (2018) [59]	26.8M	23.3
ACNet (2019) [71]	19.8M	23.8
DenseNAS-R2 (2020) [72]	19.5M	24.2
ECA-Net (2020) [73]	24.4M	22.5
ViT-B/16 (2020) [74]	86.4M	20.2
Proposed (k=180, depth=41)	27.9M	22.9 ± 0.06

The errors of compared models are reported by the official implementation.

of saliency maps that are based on gradients. What's more, in the proposed topology, shortcuts directly connect the final layer with all previous layers, which is even more desirable in conveying gradients to the input. Consequently, the saliency map of the proposed topology should be more accurate and sharper. Our overarching hypothesis is that shortcuts provide additional paths that enable a more accurate and easier gradient propagation, thereby promoting the quality of saliency maps that are based on gradients.

We use FullGrad method [78] to derive saliency maps because it can satisfy two characteristics (dependence and completeness) that the community has deemed important, but other classic methods such as SmoothGrad [79], IntegratedGrad [80], and so on cannot. Dependence describes that a feature is important if it can substantially affect the model output, while completeness is that the individual saliency scores must add up to the model output, which ensures that the total relevance corresponds to the extent of what is detected by a model. We compare our model with classic deep learning models: VGG19 [10], SqueezeNet [81], ResNet50 [11], and DenseNet169 [12]. Our model is acquired in the ImageNet experiment in the regular model regime, while others are obtained from PyTorch library.

Saliency maps for four randomly selected ImageNet images from different models are shown in Figure 7. Visually,

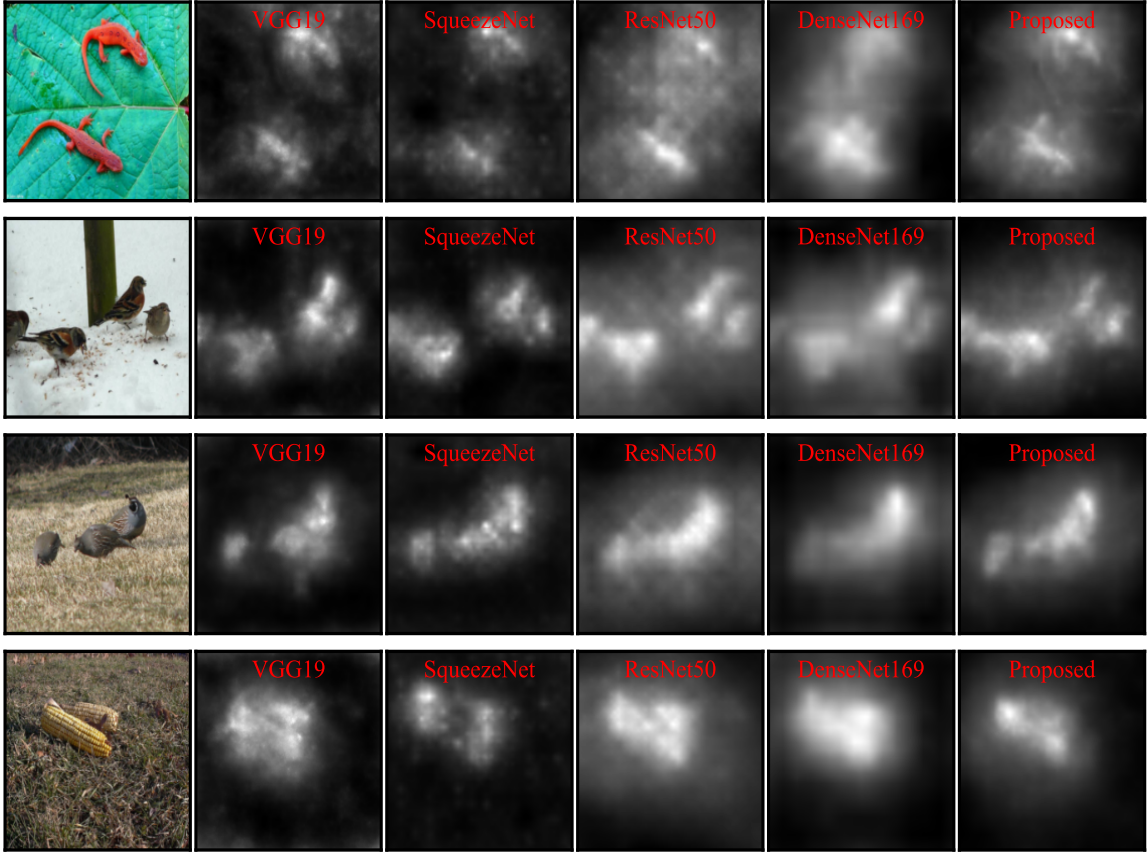


Fig. 7. Saliency maps of different models by the FullGrad method. Visually, regarding four images, saliency maps of the proposed model are sharper and their brightest points more conform to the objects.

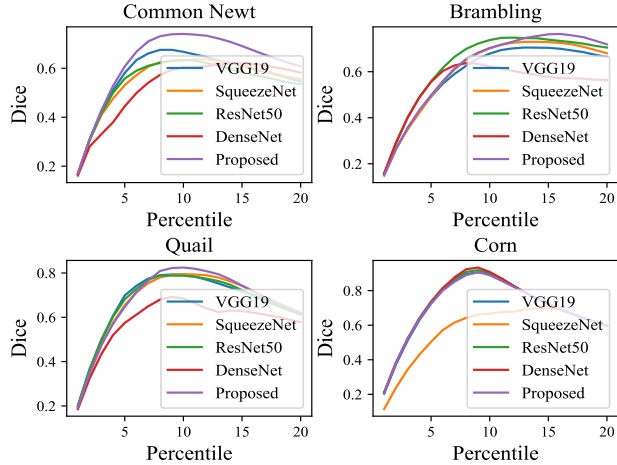


Fig. 8. Dice scores between the segmentations of an object and a saliency map with respect to the different percentile. The segmentation of a saliency map is obtained by setting the q -percentile brightest pixels as one and the rest as zero.

for all images, the saliency maps of the proposed model are sharper and the brightest points more tightly conform to the objects. In addition, we also quantitatively evaluate the quality of saliency maps. First, we threshold the saliency map by setting the q -percentile brightest pixels as one and the rest as zero to get a segmentation map. Then, we use the dice score ($\frac{2|X \cap Y|}{|X \cup Y|}$) [82] between the segmentations of an

object and a saliency map to measure their similarity. This metric by-and-large can reflect the sharpness and accuracy of a saliency map. The higher the score is, the better interpretability a model has. The obtained segmentation maps of objects and saliency maps are put in Part C of supplementary materials for conciseness. Figure 8 shows the dice scores for four objects with respect to different percentiles and models. The percentile range is from top-1% to top-20% with a step of 1%. It can be seen that the proposed model achieves the highest dice scores over common-newt, brambling, and quail images. For the corn image, the curve of the proposed model basically overlaps with those of other models.

Furthermore, we make a dataset comprising of 40 images and their segmentation maps by randomly selecting images from ImageNet validation set and manually removing their background. For each pair, we record the maximum dice score associated with certain percentile. The dice scores are shown in Table VII. Our hypothesis is verified by the fact that networks with shortcuts (the proposed, ResNet, and DenseNet) have much higher dice scores than networks without shortcuts (VGG19 and SqueezeNet). In addition, the dice score of the proposed topology is slightly better than or comparable to those of DenseNet and ResNet50.

VI. DISCUSSION

In [83], it was demonstrated that ResNet is also derived from “dense topology”. ResNet incorporates a skip-

TABLE VII
DICE SCORES OF DIFFERENT NETWORKS

Network	Dice Score
VGG19	0.609 ± 0.169
SqueezeNet	0.586 ± 0.142
ResNet50	0.629 ± 0.144
DenseNet	0.623 ± 0.149
Proposed	0.630 ± 0.161

connection as $R_l = H_l(R_{l-1}) + R_{l-1}$. Suppose $X_l = H_l(R_{l-1})$, which is the output of the l^{th} layer, and $R_0 = X_0$,

$$\begin{aligned}
 X_l &= H_l(R_{l-1}) = H_l(H_{l-1}(R_{l-2}) + R_{l-2}) \\
 &= H_l(H_{l-1}(R_{l-2}) + H_{l-2}(R_{l-3}) + R_{l-3}) \\
 &= H_l\left(\sum_{i=0}^{l-1} H_i(R_{i-1}) + R_0\right) \\
 &= H_l\left(\sum_{i=0}^{l-1} X_i + X_0\right) \\
 &= H_l(X_0 + X_1 + \dots + X_{l-1}).
 \end{aligned} \tag{35}$$

In view of such a formulation, the ResNet topology is intrinsically also the densely connected topology. Therefore, our theoretical results on the densely connected topology can be somehow extended to the ResNet topology. In [29], ResNet is interpreted as an ensemble of many paths of different lengths, and an ablation study shows that deleting individual layer does not affect the whole performance too much. In terms of ensemble behavior, as Figure 9 shown, given the depth L , there are 2^L implicit paths connecting the input and output in ResNet, while for the proposed network, the number of implicit paths is $L+1$. In addition, in ResNet, for all implicit paths, every layer has an equal chance of being passed or not passed, suggesting that each layer has an equal role. However, implicit paths of the proposed topology rely on more earlier layers than later layer. For example, in Figure 9(b), only one path connects H_2 , but three paths connect H_0 . We conduct the ablation study on the obtained networks in Table VI that are trained on ImageNet. We set the concatenation of the first layer and last layer of each block as zeros respectively and examine the performance on the test set. Because we have trained three models for the proposed topology, the ablation is repeated three times. The results are shown in Table VIII. It can be seen that undoing the first layer of each block has a significant impact, which causes only 31.84% accuracy. In contrast, the model with the last layer of each block being undone still has the classification accuracy of 61.91%, which is still better than AlexNet.

TABLE VIII
PERFORMANCE BY UNDOING DIFFERENT LAYERS

	Original	Undo Layer 1	Undo Layer 5
Accuracy (%)	77.1 ± 0.06	31.84 ± 1.81	61.91 ± 5.52

VII. CONCLUSION

In this study, we have theoretically demonstrated the expressibility and generalizability of skip connections in

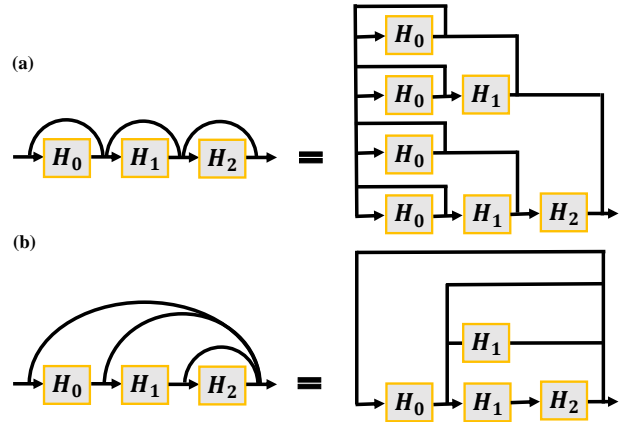


Fig. 9. (a) ResNet and its unraveled view; (b) the proposed topology and its unraveled view.

deep learning, with an emphasis on the proposed topology. Then, we have performed comprehensive prediction and classification experiments to corroborate our theoretical findings that the networks of the proposed topology enjoy a good expressibility and generalizability. We have shared our code in <https://github.com/FengleiFan/SparseShortcutTopology>. Furthermore, we have also showed the improved interpretability embraced by the proposed model in terms of saliency maps and layer importance. Future research directions can be put into exploring the utility of network equivalency in neural architecture search studies.

REFERENCES

- [1] Y. LeCun, Y. Bengio, and G. Hinton, “Deep learning,” *nature*, vol. 521, no. 7553, pp. 436–444, 2015.
- [2] G. E. Dahl, D. Yu, L. Deng, and A. Acero, “Context-dependent pre-trained deep neural networks for large-vocabulary speech recognition,” *IEEE Transactions on audio, speech, and language processing*, vol. 20, no. 1, pp. 30–42, 2011.
- [3] A. Kumar, O. Irsay, P. Ondruska, M. Iyyer, J. Bradbury, I. Gulrajani, V. Zhong, R. Paulus, and R. Socher, “Ask me anything: Dynamic memory networks for natural language processing,” in *International conference on machine learning*, pp. 1378–1387, PMLR, 2016.
- [4] H. Chen, Y. Zhang, M. K. Kalra, F. Lin, Y. Chen, P. Liao, J. Zhou, and G. Wang, “Low-dose ct with a residual encoder-decoder convolutional neural network,” *IEEE transactions on medical imaging*, vol. 36, no. 12, pp. 2524–2535, 2017.
- [5] G. Wang, “A perspective on deep imaging,” *IEEE Access*, vol. 4, pp. 8914–8924, 2016.
- [6] M. Anthimopoulos, S. Christodoulidis, L. Ebner, A. Christe, and S. Mougiakakou, “Lung pattern classification for interstitial lung diseases using a deep convolutional neural network,” *IEEE transactions on medical imaging*, vol. 35, no. 5, pp. 1207–1216, 2016.
- [7] A. Krizhevsky, I. Sutskever, and G. E. Hinton, “Imagenet classification with deep convolutional neural networks,” *Advances in neural information processing systems*, vol. 25, pp. 1097–1105, 2012.
- [8] C. Szegedy, V. Vanhoucke, S. Ioffe, J. Shlens, and Z. Wojna, “Rethinking the inception architecture for computer vision,” in *Proceedings of the IEEE conference on computer vision and pattern recognition*, pp. 2818–2826, 2016.
- [9] M. Lin, Q. Chen, and S. Yan, “Network in network,” *International Conference on Learning Representations*, 2014.
- [10] K. Simonyan and A. Zisserman, “Very deep convolutional networks for large-scale image recognition,” *International Conference on Learning Representations*, 2015.
- [11] K. He, X. Zhang, S. Ren, and J. Sun, “Deep residual learning for image recognition,” in *Proceedings of the IEEE conference on computer vision and pattern recognition*, pp. 770–778, 2016.

[12] G. Huang, Z. Liu, L. Van Der Maaten, and K. Q. Weinberger, "Densely connected convolutional networks," in *Proceedings of the IEEE conference on computer vision and pattern recognition*, pp. 4700–4708, 2017.

[13] X. Chu, B. Zhang, H. Ma, R. Xu, and Q. Li, "Fast, accurate and lightweight super-resolution with neural architecture search," *arXiv preprint arXiv:1901.07261*, 2019.

[14] B. Hariharan, P. Arbeláez, R. Girshick, and J. Malik, "Hypercolumns for object segmentation and fine-grained localization," in *Proceedings of the IEEE conference on computer vision and pattern recognition*, pp. 447–456, 2015.

[15] V. Badrinarayanan, A. Kendall, and R. Cipolla, "Segnet: A deep convolutional encoder-decoder architecture for image segmentation," *IEEE transactions on pattern analysis and machine intelligence*, vol. 39, no. 12, pp. 2481–2495, 2017.

[16] R. K. Srivastava, K. Greff, and J. Schmidhuber, "Training very deep networks," in *Proceedings of the 28th International Conference on Neural Information Processing Systems-Volume 2*, pp. 2377–2385, 2015.

[17] G. Larsson, M. Maire, and G. Shakhnarovich, "Fractalnet: Ultra-deep neural networks without residuals," *International Conference on Learning Representations*, 2017.

[18] K.-I. Funahashi, "On the approximate realization of continuous mappings by neural networks," *Neural networks*, vol. 2, no. 3, pp. 183–192, 1989.

[19] K. Hornik, M. Stinchcombe, and H. White, "Multilayer feedforward networks are universal approximators," *Neural networks*, vol. 2, no. 5, pp. 359–366, 1989.

[20] L. Szymanski and B. McCane, "Deep networks are effective encoders of periodicity," *IEEE transactions on neural networks and learning systems*, vol. 25, no. 10, pp. 1816–1827, 2014.

[21] D. Rolnick and M. Tegmark, "The power of deeper networks for expressing natural functions," *International Conference on Learning Representations*, 2018.

[22] H. N. Mhaskar and T. Poggio, "Deep vs. shallow networks: An approximation theory perspective," *Analysis and Applications*, vol. 14, no. 06, pp. 829–848, 2016.

[23] R. Eldan and O. Shamir, "The power of depth for feedforward neural networks," in *Conference on learning theory*, pp. 907–940, PMLR, 2016.

[24] S. Liang and R. Srikant, "Why deep neural networks for function approximation?," in *International Conference on Learning Representations*, 2017.

[25] V. Tikhomirov, "On the representation of continuous functions of several variables as superpositions of continuous functions of one variable and addition," in *Selected Works of AN Kolmogorov*, pp. 383–387, Springer, 1991.

[26] Z. Lu, H. Pu, F. Wang, Z. Hu, and L. Wang, "The expressive power of neural networks: a view from the width," in *Proceedings of the 31st International Conference on Neural Information Processing Systems*, pp. 6232–6240, 2017.

[27] F. Fan, J. Xiong, and G. Wang, "Universal approximation with quadratic deep networks," *Neural Networks*, vol. 124, pp. 383–392, 2020.

[28] H. Lin and S. Jegelka, "Resnet with one-neuron hidden layers is a universal approximator," *Advances in Neural Information Processing Systems*, vol. 31, pp. 6169–6178, 2018.

[29] A. Veit, M. Wilber, and S. Belongie, "Residual networks behave like ensembles of relatively shallow networks," in *Proceedings of the 30th International Conference on Neural Information Processing Systems*, pp. 550–558, 2016.

[30] T. L. Liu, M. Chen, M. Zhou, S. Du, E. Zhou, and T. Zhao, "Towards understanding the importance of shortcut connections in residual networks," *Advances in neural information processing systems*, 2019.

[31] F. He, T. Liu, and D. Tao, "Why resnet works? residuals generalize.," *IEEE transactions on neural networks and learning systems*, vol. 31, pp. 5349–5362, 2020.

[32] E. Kang, H. J. Koo, D. H. Yang, J. B. Seo, and J. C. Ye, "Cycle-consistent adversarial denoising network for multiphase coronary ct angiography," *Medical physics*, vol. 46, no. 2, pp. 550–562, 2019.

[33] C. You, G. Li, Y. Zhang, X. Zhang, H. Shan, M. Li, S. Ju, Z. Zhao, Z. Zhang, W. Cong, *et al.*, "Ct super-resolution gan constrained by the identical, residual, and cycle learning ensemble (gan-circle)," *IEEE transactions on medical imaging*, vol. 39, no. 1, pp. 188–203, 2019.

[34] B. Hamann and J.-L. Chen, "Data point selection for piecewise linear curve approximation," *Computer Aided Geometric Design*, vol. 11, no. 3, pp. 289–301, 1994.

[35] L. Zhu, R. Deng, M. Maire, Z. Deng, G. Mori, and P. Tan, "Sparsely aggregated convolutional networks," in *Proceedings of the European Conference on Computer Vision (ECCV)*, pp. 186–201, 2018.

[36] J. Schmidt-Hieber, "The kolmogorov–arnold representation theorem revisited," *Neural Networks*, vol. 137, pp. 119–126, 2021.

[37] P. L. Bartlett, D. J. Foster, and M. Telgarsky, "Spectrally-normalized margin bounds for neural networks," in *Proceedings of the 31st International Conference on Neural Information Processing Systems*, pp. 6241–6250, 2017.

[38] B. Neyshabur, R. Tomioka, and N. Srebro, "Norm-based capacity control in neural networks," in *Conference on Learning Theory*, pp. 1376–1401, PMLR, 2015.

[39] B. Neyshabur, S. Bhojanapalli, and N. Srebro, "A pac-bayesian approach to spectrally-normalized margin bounds for neural networks," in *International Conference on Learning Representations*, 2018.

[40] L. Wu, C. Ma, and W. E, "How sgd selects the global minima in over-parameterized learning: A dynamical stability perspective," in *Proceedings of the 32nd International Conference on Neural Information Processing Systems*, pp. 8289–8298, 2018.

[41] Z. Allen-Zhu, Y. Li, and Y. Liang, "Learning and generalization in overparameterized neural networks, going beyond two layers," *arXiv preprint arXiv:1811.04918*, 2018.

[42] A. Brutzkus, A. Globerson, E. Malach, and S. Shalev-Shwartz, "Sgd learns over-parameterized networks that provably generalize on linearly separable data," in *International Conference on Learning Representations*, 2018.

[43] B. Neyshabur, Z. Li, S. Bhojanapalli, Y. LeCun, and N. Srebro, "The role of over-parametrization in generalization of neural networks," in *International Conference on Learning Representations*, 2018.

[44] P. Nakkiran, G. Kaplun, Y. Bansal, T. Yang, B. Barak, and I. Sutskever, "Deep double descent: Where bigger models and more data hurt," in *International Conference on Learning Representations*, 2019.

[45] V. Vovk, "Kernel ridge regression," in *Empirical inference*, pp. 105–116, Springer, 2013.

[46] A. Jacot, F. Gabriel, and C. Hongler, "Neural tangent kernel: Convergence and generalization in neural networks," in *Advances in neural information processing systems*, pp. 8571–8580, 2018.

[47] S. Arora, S. S. Du, W. Hu, Z. Li, R. R. Salakhutdinov, and R. Wang, "On exact computation with an infinitely wide neural net," in *Advances in Neural Information Processing Systems*, pp. 8141–8150, 2019.

[48] D. Harrison Jr and D. L. Rubinfeld, "Hedonic housing prices and the demand for clean air," *Journal of environmental economics and management*, vol. 5, no. 1, pp. 81–102, 1978.

[49] S. Ioffe and C. Szegedy, "Batch normalization: Accelerating deep network training by reducing internal covariate shift," in *International conference on machine learning*, pp. 448–456, PMLR, 2015.

[50] N. Srivastava, G. Hinton, A. Krizhevsky, I. Sutskever, and R. Salakhutdinov, "Dropout: a simple way to prevent neural networks from overfitting," *The journal of machine learning research*, vol. 15, no. 1, pp. 1929–1958, 2014.

[51] G. Huang, Y. Sun, Z. Liu, D. Sedra, and K. Q. Weinberger, "Deep networks with stochastic depth," in *European conference on computer vision*, pp. 646–661, Springer, 2016.

[52] Z. Huang, S. Liang, M. Liang, and H. Yang, "Dianet: Dense-and-implicit attention network.," in *AAAI*, pp. 4206–4214, 2020.

[53] H. Kabir, M. Abdar, S. M. J. Jalali, A. Khosravi, A. F. Atiya, S. Nahavandi, and D. Srinivasan, "Spinalnet: Deep neural network with gradual input," *arXiv preprint arXiv:2007.03347*, 2020.

[54] G. Franchi, A. Bursuc, E. Aldea, S. Dubuisson, and I. Bloch, "Encoding the latent posterior of bayesian neural networks for uncertainty quantification," *arXiv preprint arXiv:2012.02818*, 2020.

[55] M. Sandler, A. Howard, M. Zhu, A. Zhmoginov, and L.-C. Chen, "Mobilnetv2: Inverted residuals and linear bottlenecks," in *Proceedings of the IEEE conference on computer vision and pattern recognition*, pp. 4510–4520, 2018.

[56] M. Tan and Q. Le, "Efficientnet: Rethinking model scaling for convolutional neural networks," in *International Conference on Machine Learning*, pp. 6105–6114, PMLR, 2019.

[57] Y. Chen, H. Fan, B. Xu, Z. Yan, Y. Kalantidis, M. Rohrbach, S. Yan, and J. Feng, "Drop an octave: Reducing spatial redundancy in convolutional neural networks with octave convolution," in *Proceedings of the*

IEEE International Conference on Computer Vision, pp. 3435–3444, 2019.

[58] Anonymous, “Lambdanetworks: Modeling long-range interactions without attention,” in *Submitted to International Conference on Learning Representations*, 2021. under review.

[59] J. Hu, L. Shen, and G. Sun, “Squeeze-and-excitation networks,” in *Proceedings of the IEEE conference on computer vision and pattern recognition*, pp. 7132–7141, 2018.

[60] Y. Li, Z. Kuang, Y. Chen, and W. Zhang, “Data-driven neuron allocation for scale aggregation networks,” in *Proceedings of the IEEE Conference on Computer Vision and Pattern Recognition*, pp. 11526–11534, 2019.

[61] K. Han, Y. Wang, Q. Tian, J. Guo, C. Xu, and C. Xu, “Ghostnet: More features from cheap operations,” in *Proceedings of the IEEE/CVF Conference on Computer Vision and Pattern Recognition*, pp. 1580–1589, 2020.

[62] S. Xie, A. Kirillov, R. Girshick, and K. He, “Exploring randomly wired neural networks for image recognition,” in *Proceedings of the IEEE International Conference on Computer Vision*, pp. 1284–1293, 2019.

[63] J. Deng, W. Dong, R. Socher, L.-J. Li, K. Li, and L. Fei-Fei, “Imagenet: A large-scale hierarchical image database,” in *2009 IEEE conference on computer vision and pattern recognition*, pp. 248–255, Ieee, 2009.

[64] X. Zhang, X. Zhou, M. Lin, and J. Sun, “Shufflenet: An extremely efficient convolutional neural network for mobile devices,” in *Proceedings of the IEEE conference on computer vision and pattern recognition*, pp. 6848–6856, 2018.

[65] B. Zoph, V. Vasudevan, J. Shlens, and Q. V. Le, “Learning transferable architectures for scalable image recognition,” in *Proceedings of the IEEE conference on computer vision and pattern recognition*, pp. 8697–8710, 2018.

[66] E. Real, A. Aggarwal, Y. Huang, and Q. V. Le, “Regularized evolution for image classifier architecture search,” in *Proceedings of the aaai conference on artificial intelligence*, vol. 33, pp. 4780–4789, 2019.

[67] C. Liu, B. Zoph, M. Neumann, J. Shlens, W. Hua, L.-J. Li, L. Fei-Fei, A. Yuille, J. Huang, and K. Murphy, “Progressive neural architecture search,” in *Proceedings of the European Conference on Computer Vision (ECCV)*, pp. 19–34, 2018.

[68] H. Liu, K. Simonyan, and Y. Yang, “Darts: Differentiable architecture search,” in *International Conference on Learning Representations*, 2018.

[69] B. Wu, X. Dai, P. Zhang, Y. Wang, F. Sun, Y. Wu, Y. Tian, P. Vajda, Y. Jia, and K. Keutzer, “Fbnet: Hardware-aware efficient convnet design via differentiable neural architecture search,” in *Proceedings of the IEEE Conference on Computer Vision and Pattern Recognition*, pp. 10734–10742, 2019.

[70] I. Radosavovic, R. P. Kosaraju, R. Girshick, K. He, and P. Dollár, “Designing network design spaces,” in *Proceedings of the IEEE/CVF Conference on Computer Vision and Pattern Recognition*, pp. 10428–10436, 2020.

[71] G. Wang, K. Wang, and L. Lin, “Adaptively connected neural networks,” in *Proceedings of the IEEE Conference on Computer Vision and Pattern Recognition*, pp. 1781–1790, 2019.

[72] J. Fang, Y. Sun, Q. Zhang, Y. Li, W. Liu, and X. Wang, “Densely connected search space for more flexible neural architecture search,” in *Proceedings of the IEEE/CVF Conference on Computer Vision and Pattern Recognition*, pp. 10628–10637, 2020.

[73] Q. Wang, B. Wu, P. Zhu, P. Li, W. Zuo, and Q. Hu, “Eca-net: Efficient channel attention for deep convolutional neural networks,” in *Proceedings of the IEEE/CVF Conference on Computer Vision and Pattern Recognition*, pp. 11534–11542, 2020.

[74] A. Dosovitskiy, L. Beyer, A. Kolesnikov, D. Weissenborn, X. Zhai, T. Unterthiner, M. Dehghani, M. Minderer, G. Heigold, S. Gelly, *et al.*, “An image is worth 16x16 words: Transformers for image recognition at scale,” *arXiv preprint arXiv:2010.11929*, 2020.

[75] F. Fan, J. Xiong, M. Li, and G. Wang, “On interpretability of artificial neural networks: A survey,” *arXiv preprint arXiv:2001.02522*, 2020.

[76] B.-J. Hou and Z.-H. Zhou, “Learning with interpretable structure from gated rnn,” *IEEE transactions on neural networks and learning systems*, vol. 31, no. 7, pp. 2267–2279, 2020.

[77] A. B. Arrieta, N. Díaz-Rodríguez, J. Del Ser, A. Bennetot, S. Tabik, A. Barbado, S. García, S. Gil-López, D. Molina, R. Benjamins, *et al.*, “Explainable artificial intelligence (xai): Concepts, taxonomies, op- portunities and challenges toward responsible ai,” *Information Fusion*, vol. 58, pp. 82–115, 2020.

[78] S. Srinivas and F. Fleuret, “Full-gradient representation for neural network visualization,” in *Advances in Neural Information Processing Systems*, pp. 4124–4133, 2019.

[79] D. Smilkov, N. Thorat, B. Kim, F. Viégas, and M. Wattenberg, “Smoothgrad: removing noise by adding noise,” *International conference on machine learning*, 2017.

[80] M. Sundararajan, A. Taly, and Q. Yan, “Axiomatic attribution for deep networks,” *International conference on machine learning*, 2017.

[81] F. N. Iandola, S. Han, M. W. Moskewicz, K. Ashraf, W. J. Dally, and K. Keutzer, “SqueezeNet: Alexnet-level accuracy with 50x fewer parameters and< 0.5 mb model size,” *International Conference on Learning Representations*, 2017.

[82] L. R. Dice, “Measures of the amount of ecologic association between species,” *Ecology*, vol. 26, no. 3, pp. 297–302, 1945.

[83] W. Wang, X. Li, T. Lu, and J. Yang, “Mixed link networks,” in *Proceedings of the 27th International Joint Conference on Artificial Intelligence*, pp. 2819–2825, 2018.